Colloid Polym Sci (2016) 294:1463–1473
DOI 10.1007/s00396-016-3907-6

ORIGINAL CONTRIBUTION

Rheological behavior of poly(acrylonitrile) concentrated solutions: effect of Sb_2O_3 nanoparticles on shear and extensional flow

Omid Akhlaghi[1] · **Yusuf Z. Menceloglu**[1] · **Ozge Akbulut**[1]

Received: 11 March 2016 / Revised: 13 June 2016 / Accepted: 13 June 2016 / Published online: 23 June 2016

Abstract This study investigates the effect of antimony trioxide (Sb_2O_3) nanoparticles on shear and extensional flow properties of concentrated polyacrylonitrile (PAN) solutions. Through shear rheology, a wide variety of rheological observations, such as Payne effect, applicability of Cox–Merz rule, and range of linear viscoelastic behavior (critical strain) were assessed. The presence of Sb_2O_3 nanoparticles was found to promote the non-linear viscoelasticity of the solutions and give rise to enhanced heterogeneous domains of PAN in the solution. In elongational flow, thinning dynamics of the nanocomposites was tracked to reproduce the dynamics of deformation in the spinline of the dry-jet wet spinning process. Increasing amounts of Sb_2O_3 nanoparticles in the solution were shown to improve the lifetime of the filament. All solutions were ruptured through elastocapillary behavior, while strengthened strain-hardening behavior was observed after the addition of Sb_2O_3 nanoparticles to the polymer solution.

Keywords Capillary breakup extensional rheometry · Polyacrylonitrile · Nanocomposite · Rheology

Introduction

Halogenated flame retardants are frequently incorporated to engineering plastics due to their effectiveness at low doping amounts. Antimony oxides, particularly Sb_2O_3, were shown to produce a synergistic effect when used with this type of flame retardants [1–3]. Notably, Sb_2O_3 is also effective in the halogen-free systems such as ammonium polyphosphate/polypropylene [4] and aluminum diethlyphosphinate/polyethylene terephthalate [5]. Flame retardants can be added to polymer melts or solutions during the production of fibers prior to extrusion process to manufacture synthetic fibers. These fibers are referred to as inherently flame retardant.

Poly(acrylonitrile) (PAN) has found various applications in textile industry and in the production of high-performance carbon fibers [6, 7]. Despite good stability and mechanical properties, PAN and its copolymers decompose rapidly under burning conditions and produce flammable volatiles [8]. Recently, considerable efforts have been devoted to the development of novel PAN processing techniques and fiber-forming technologies [9–11]. Moreover, extensive studies have been reported on the preparation of PAN nanocomposites with different nanoparticles to improve mechanical, electrical, and optical properties of the final products [7, 12–14]. However, there are few studies focusing on the processability of PAN solutions particularly when they are doped with nanostructured components [9, 15, 16]. Dry-jet wet spinning is the most widely used method for the production of PAN fibers [17]. In this process, polymer solution is extruded through a spinneret and stretched to the desired diameter in an air gap before a coagulation bath to form a stable spinline. Due to the close relationship between processability and viscoelastic behavior of polymer solutions, understanding the rheological behavior of PAN solutions is crucial for the design of processing and fiber-forming technologies [7, 18]. In order to reproduce the rheological response of a solution in the spinning process, concomitant investigation of shear and

✉ Ozge Akbulut
ozgeakbulut@sabanciuniv.edu

[1] Faculty of Engineering and Natural Sciences, Sabanci University, Istanbul 34956, Turkey

elongational flow behavior is necessary. The former provides the precise control of flow rates in the extrusion step, and the latter simulates the behavior of the solution in the spinline [19].

Here, we studied the influence of Sb_2O_3 nanoparticles on the shear and extensional rheological behavior of PAN solution at an industrially relevant concentration of the polymer. Since the amount of synergist is normally lower than 10 phr (<9 wt% compared to dry mass of polymer) [1, 8, 20], therefore, we focused on PAN solutions with low Sb_2O_3 content (1–8 wt% relative to PAN content). We, first, characterized the rheological properties in shear mode and demonstrated the enhancement of elasticity and physical structures of the solutions with additive content. The extensional response of the system, then, was monitored by capillary breakup extensional rheometery. We found that increasing amount of Sb_2O_3 content improves the lifetime of the filament and shifts the flow behavior of solutions toward that of a Newtonian fluid.

Materials and methods

Starting materials

Sb_2O_3 powder with a diameter of <250 nm and dimethylacetamide (DMAc, >99 %) were purchased from Sigma-Aldrich and Merck Schuchardt (Germany), respectively. PAN powder with comonomer content of 93 % acrylonitrile and 7 % vinyl acetate, average molecular weight of 2.7×10^5 g/mol and molecular weight distribution (M_w/M_n) of 3.17 received by the courtesy of a fiber-manufacturer company, AKSA. PAN powders were vacuum-dried at 70 °C for 3 days and sealed to avoid adsorption of humidity. Sb_2O_3 powder, DMAc, and PAN powders were used without further purification.

Sample preparation

PAN powder was first dissolved in DMAc to obtain 1 wt% PAN solution, and then, different amounts of Sb_2O_3 were added to this dilute polymer solution. These suspensions were stirred for 2 h at 80 °C in sealed containers. Subsequently, polymer concentration was increased to 20 wt% by gradual addition of PAN powder to the system at 80 °C in 6 h. Afterwards, the mixture was stirred for additional 6 h to produce optically homogenous Sb_2O_3-PAN/DMAc solutions. The suspensions contained 1, 2, 4, and 8 wt% Sb_2O_3 compared to PAN powder, and the total amount of solid content (PAN and nanoparticles) ranged between 20.1 and 21 wt%. The suspensions hereafter named as S1, S2, S4, and S8, respectively. The neat polymer solution is referred to as S0.

Characterization methods

The linear and non-linear rheological measurements in shear mode were conducted in Anton-Paar MCR 302 rheometer with cone-plate geometry of 50 mm/2° and a gap size of 0.208 mm. After loading each sample, a thin layer of low-viscosity paraffin oil was employed around the outer edge of the plates to protect the sample from adsorption of humidity. Temperature was set to 25 °C, and all samples remained uninterrupted for 60 s before starting the measurement. In steady-state tests, the shear rate ranged from 0.1 to 100 s^{-1}. In dynamic regime, frequency was set to 10 rad s^{-1} and strain was changed from 0.01 to 1000 % to find the range of linear viscoelastic region. For the frequency sweep tests, strain was maintained at 10 % and frequency was swept from 0.1 to 100 rad s^{-1}. A new sample is used for each test.

The extensional properties of PAN-Sb_2O_3 solutions were assessed by using a capillary breakup extensional rheometer (HAAKE CaBER 1, Thermo Scientific, Germany) with two 6-mm-diameter plates. A fluid drop (~0.06 ml) was placed between two plates and then exposed to an extensional step strain. After establishment of the liquid bridge, the midpoint diameter ($D(t)$) was monitored as a function of time using a laser micrometer. Plate separation was changed from $L_0 = 1.99$ mm to $L_f = 12$ mm within 50 ms. Therefore, the extension rate ($\dot{\varepsilon}$) was set to 35.93 s^{-1} according to the relation $L_f = L_0 \exp(\dot{\varepsilon} t)$, where t is time (s). In order to minimize the gravitational sagging, initial separation of 1.99 mm was chosen to be less than the capillary length $L_{cap} = (\sigma/\rho g)^{1/2}$, where σ (mN m^{-1}) and $\rho = 0.99$ g cm^{-3} are the surface tension and density of polymer solution, respectively, and $g = 9.81$ m s^{-2} is the standard acceleration due to gravity. Surface tension of polymer solutions was measured to be $\sigma = 40$ mN m^{-1} in a KSV Sigma 701 tensiometer; thus, L_{cap} was calculated as ~2.03 mm.

Distribution of Sb_2O_3 nanoparticles in polymer matrix was monitored using Leo Supra 35VP field emission scanning electron microscope at acceleration voltage of 10 KeV. Nanocomposite films were prepared by dipping the glass substrates into PAN-Sb_2O_3 nanocomposite solutions immediately after cessation of mixing process. The substrates were vacuum-dried at 70 °C for 24 h and sputter-coated with carbon.

The nuclear magnetic resonance (NMR) spin-spin relaxation (T2) test was performed in a Varian Unity Inova 500 MHz spectrometer at room temperature to assess the mobility of the polymer chains in the solution. All measurements were performed using the pulse spacing of 5–20 ms and 23 data points were collected by sampling the echo maxima.

Thermogravimetrical analysis (TGA, Netzsch STA 449C Jupiter thermal analyzer) on neat polymer solution and nanocomposites was carried out by heating up ~10 mg samples at 10 K/min from room temperature to 300 °C under nitrogen atmosphere.

Results and discussion

Shear rheology

Dynamic strain sweep measurements were carried out to quantify the viscoelastic nature of solutions and determine the crossover strain from linear to non-linear viscoelasticity. As shown in Fig. 1a, at low strains, storage modulus (G') is independent of the applied strain suggesting that the solutions are in the linear viscoelastic regime. When the strain amplitude grows, a sudden drop was observed after a critical strain (γ_c), which is marked as the transition from linear to non-linear viscoelasticity. Addition of Sb_2O_3 nanoparticles to polymer solution changed γ_c from 26.6 % in S0 to 23–25 % in S1–S8 nanocomposites (Table 1).

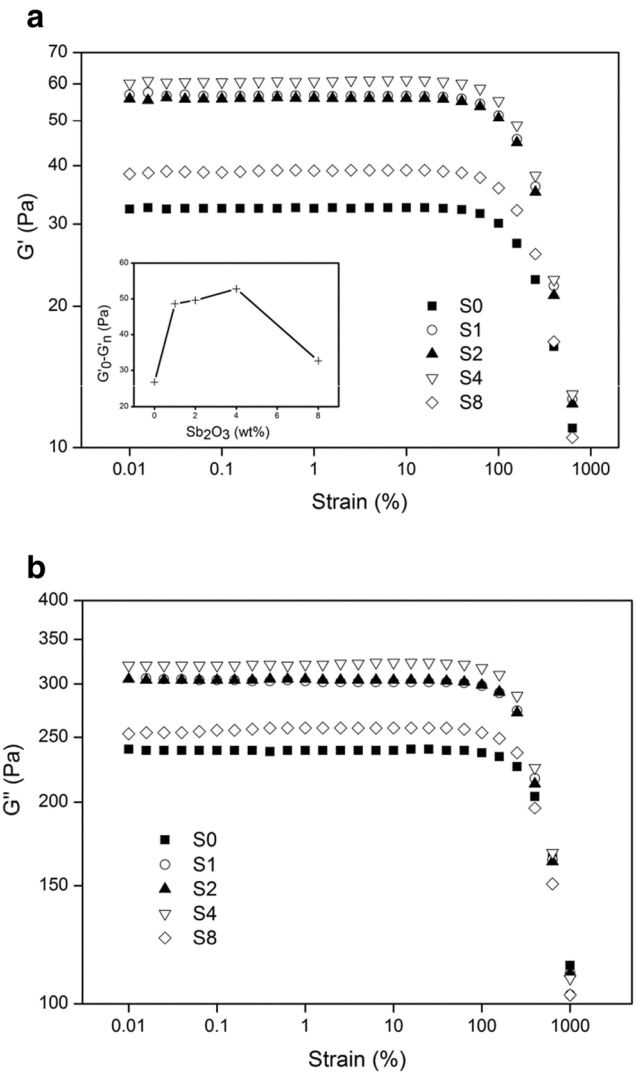

Fig. 1 Strain dependence of **a** storage modulus and **b** loss modulus at a fixed frequency of $\omega = 10$ rad s^{-1} (*inset* shows the difference between finite-strain rubbery plateau modulus, G'_0, and elastic modulus at high strain amplitude, G'_n)

Table 1 Zero-shear rate viscosity of solutions, slope of Cole–Cole plot, and critical strain for transition from linear to non-linear viscoelasticity

	η_0 (Pa s)	Slope of G'–G''plot	γ_c (%)
S0	26.0	1.78	26.6
S1	28.8	1.75	23.2
S2	34.7	1.70	23.4
S4	36.9	1.67	23.9
S8	27.8	1.75	25.4

In general, strain amplitude dependence of dynamic viscoelastic behavior of filled polymers is known as Payne effect. This effect is quantitatively defined as the difference between finite-strain rubbery plateau modulus G'_0 ($G'\gamma \rightarrow 0$) and the lowest level of G' at high strain amplitude (G'_n) [21]. Incorporation of Sb_2O_3 nanoparticles into PAN solution increases G'_0 and promotes the non-linear viscoelasticity in solutions (G'_0–G'_n) as shown in inset of Fig. 1a. In addition, similar trend was observed for the dependence of loss modulus (G'') on strain amplitude (Fig. 1b) as the G'' plateau is increased with Sb_2O_3 content. These types of behaviors are in agreement with the previous reports on strain amplitude dependence of polymer nanocomposites in solution or melt state [22, 23]. According to Cassagnau [21, 24], the non-linear behavior of filled polymer solutions can be correlated with filler–filler interactions (e.g., agglomeration-deagglomeration of fillers or breakdown of the filler network), filler–polymer interactions (e.g., trapping of polymer chains), and disentanglement of polymer chains. In order to clarify the origin of non-linear viscoelastic behavior, the dynamic oscillatory rheology was performed on nanocomposites (Fig. 2a).

Generally, G' and G'' increase with frequency and show a plateau modulus at high frequencies. The latter phenomenon demonstrates a typical solid-like behavior of polymer solutions that is attributed to the short times available for PAN chains to rearrange and/or relax at high frequencies [25]. On the other hand, observation of a plateau of G' at low frequencies and frequency-independent state of loss factor (tan δ) illustrates the formation of a filler network in the nanocomposite solutions [26]. As shown in Fig. 2a, in the terminal region of S0, the slope of log G' versus log ω and log G″ versus log ω is close to 2 and 1, respectively, in agreement with the behavior of relaxed polymer chains [23, 27]. After the introduction of Sb_2O_3 nanoparticles, G' remains lower than G'' independent of the frequency, and no plateau is noticed at low frequencies. As shown in Fig. 2b, the curves of tan δ are slowly depressed with increasing amounts of filler but not close to the frequency-independent state, referred to as "gel state." Therefore, we can conclude that all nanocomposites showed liquid-like behavior ($G'' > G'$) [22, 23] at 25 °C with no sign of formation of 3D network in solutions. To further

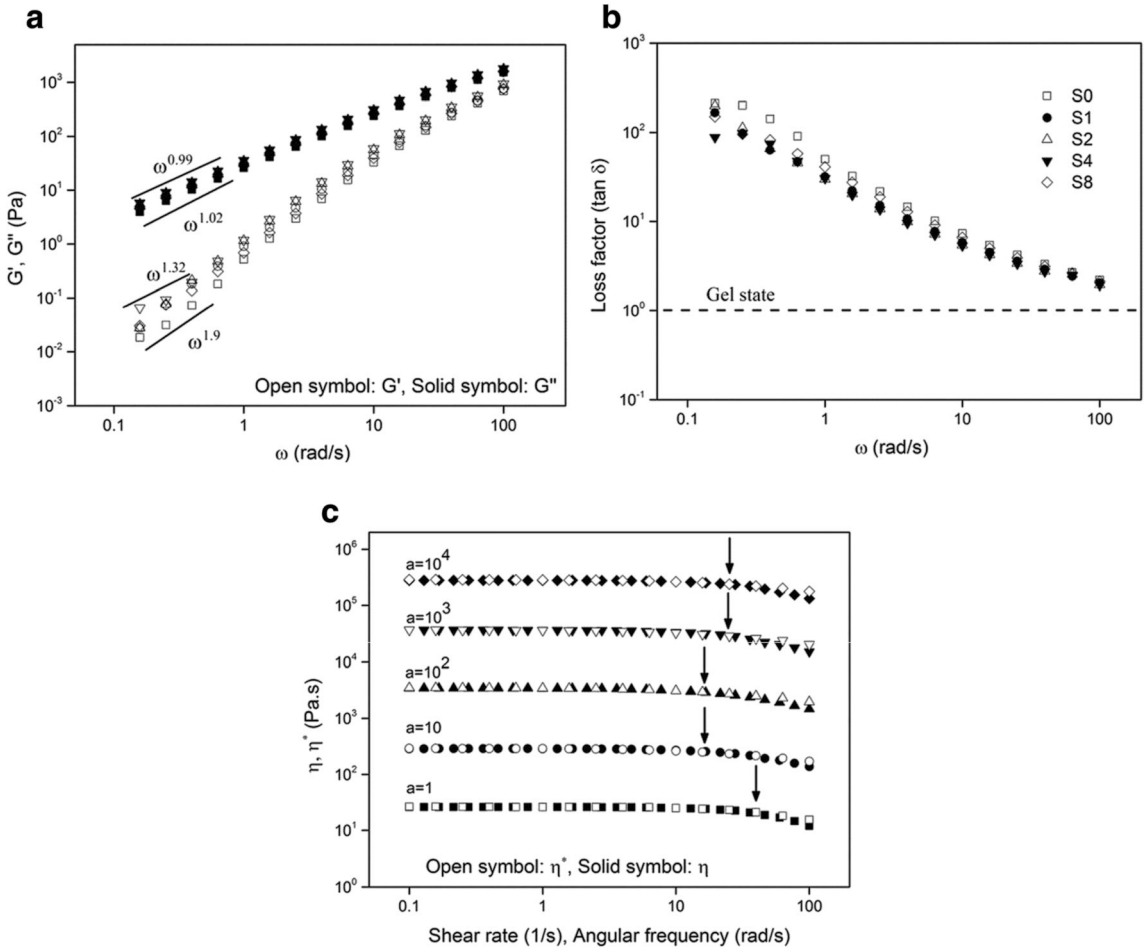

Fig. 2 **a** Storage modulus (G') and loss modulus (G''), **b** loss factor (tan δ) as a function of frequency, and **c** rate dependence of steady and dynamic viscosity of neat polymer solution and its nanocomposites (data were shifted along the vertical axes by factor of **a** to avoid overlapping; curves from bottom to top are S0, S1, S2, S4, and S8)

support the liquid-like behavior of the solutions, the non-existence of gel network (particularly weak gel network) was proved by applicability of Cox–Merz rule. The steady shear viscosity (η) and the magnitude of the complex viscosity ($|\eta^*|$) of entangled polymer solutions are suggested to overlap closely at equivalent values of shear rate (1/s) and frequency (rad/s) (semi-empirical Cox–Merz rule) [28]. When weak gel networks are present in the system, $|\eta^*|$ becomes higher than η, since these networks can survive small oscillatory deformations but not large steady shear deformations. As shown in Fig. 2c, the rate dependence of steady shear viscosity is in good agreement with frequency dependence of dynamic viscosity of polymer solutions. Indeed, η and η^* curves were superimposible till high shear rates indicating that the absence of weak gel structure in the solutions. However, after a critical point, marked by the arrows in Fig. 2c, all solutions tend to depart from the Cox–Merz rule. As all solutions display the same deviation from the Cox–Merz rule, it can be concluded that addition of Sb_2O_3 nanoparticles does not considerably disturb the structure of polymer solution. Besides, observation of earlier critical shear rates in the nanocomposites compared to the neat polymer solution reveals the promotion of the disentanglement of the polymer chains in the presence of nanoparticles. Likely, the orientation of nanoparticles under steady shear deformation has been suggested to facilitate disentanglement of polymer chains, while this effect may not be detectable under dynamic shear mode [25].

To investigate the interaction between polymer chains and fillers in solution, the segmental mobility of polymer chains in the presence of Sb_2O_3 nanoparticles was examined by measuring NMR spin-spin relaxation times (T2). The normalized relaxation curves at 25 °C were shown in Fig. 3a. Sb_2O_3 nanoparticles were observed to decrease the mobility of the polymer chains as shown by the shift of the relaxation curves to the left (shorter T2). This result suggests that trapping of polymer chains on the particles is likely to occur, and presence of filler reinforces the polymer chains in the solution [29]. This reinforcement effect of Sb_2O_3 nanoparticles on polymer chains was also manifested by the change in dynamic

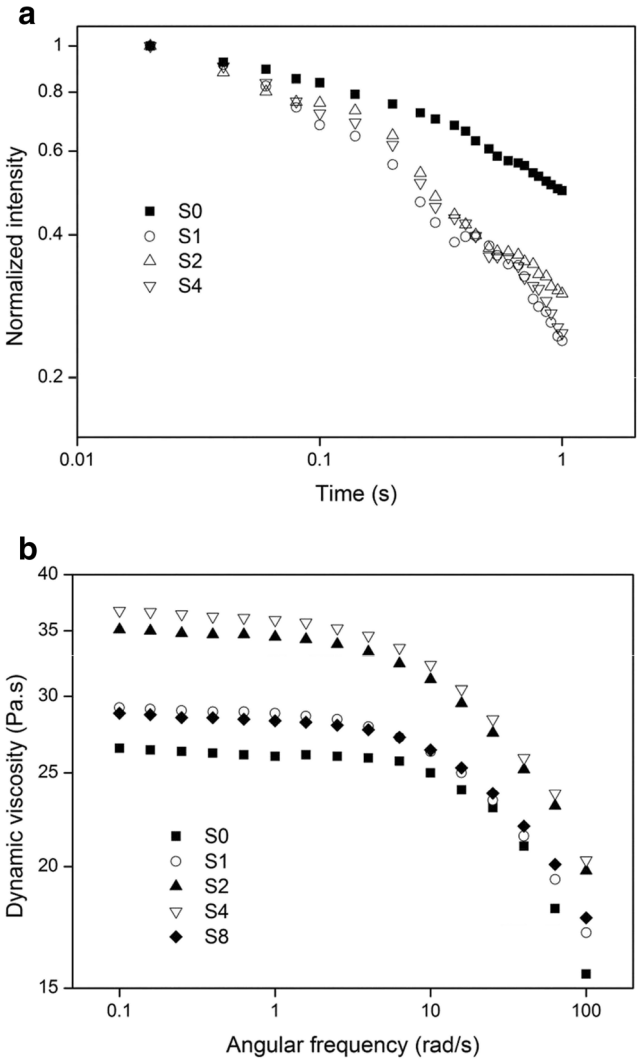

Fig. 3 **a** Normalized NMR spin–spin relaxation times of PAN solutions with different amounts of Sb_2O_3 nanoparticles and **b** dynamic viscosity as a function of angular frequency

viscosity. As shown in Fig. 3b and Table 1, viscosity of nanocomposites increased with filler content up to 4 wt% and decreased beyond this point but not to lower values of the neat polymer solution.

Rheological characterization, particularly dynamic properties, is frequently used as an indirect method to evaluate the heterogeneous domains in highly polar systems and also dispersion state of fillers in polymer nanocomposites [30–32]. In the former, frequency dependence of G'' can reveal presence and strength of heterogeneous domains in polymer solutions. In the latter, an increase of G' and η^* in low-frequency regime is linked to attractive interfacial interactions of polymer–filler and/or better dispersion of the filler in the polymer matrix [30]. As shown in Figs. 2a and 3b, progressive improvement of G' and η^* by filler content up to 4 wt% can be attributed to well-dispersed filler particles in nanocomposites, while observation of sudden drop in dynamic properties of S8 compared to S4 shows reduction of polymer–filler interactions and poor dispersion of the filler in PAN matrix. Figure 4a–c displays the scanning electron microscopy (SEM) of nanocomposite films. Sb_2O_3 nanoparticles in S1 and S4 are completely dispersed in the polymer matrix. On the other hand, agglomerated nanoparticles are more frequently observed in the nanocomposite with 8 wt% filler (S8, Fig. 4c) that is in agreement with the results of dynamic rheology. Figure 4d, e shows SEM of S4 and S8 in higher magnification, respectively, that visualization confirms the effective dispersion at 4 wt% and agglomeration at 8 wt% filler content.

Figure 5a displays the $G''^{1/2}$ as a function of $\omega^{1/2}$ for PAN solutions with different amounts of Sb_2O_3 nanoparticles. Strength of heterogeneous domains can be determined by the value of yield stress—the minimum energy required to break this physical structure and obtained by modified Casson plot defined by Eq. 1 [32, 33]:

$$G''^{1/2} = G_y''^{1/2} + K\omega^{1/2} \quad (1)$$

where G_y'' stands for yield stress (Pa), K is a constant, and ω is angular frequency (rad s^{-1}). Non-zero intercept of S0 indicates the existence of a physical structure in the neat polymer solution, while addition of Sb_2O_3 nanoparticles increased G_y'' and strengthened this physical structure.

To further support the heterogeneity of solutions, the Cole–Cole plot (logarithmic plot of G' versus G'') was shown in Fig. 5b. Perfectly homogeneous polymer solution or melt without any physical structure gives a slope of 2 in Cole–Cole plots, whereas values lower than 2 indicate the formation of heterogeneous structures [33, 34]. All curves in Fig. 5b displayed a slope of less than 2, while addition of nanoparticles led to a decline of the slope of the curve (Table 1). Overall, these results suggest that addition of Sb_2O_3 nanoparticles promotes the formation of heterogeneous domains in PAN solutions. This formation in concentrated solutions of PAN originates from permanent dipole of nitrile side group in PAN monomer units [35]. Strengthening of these physical structures by addition of Sb_2O_3 nanoparticles potentially arises from resonance charge distribution in DMAc molecules that can decrease the polarization consistency and thus tolerance of PAN chains to environmental conditions [32, 36]. As a result, the presence of the filler would weaken the interactions of PAN-DMAc, and the polarized solvent molecules that are oriented between PAN nitrile groups (solvent bridge) may be kicked out to form a shorter bridge (bound solvent). Thus, PAN chains that are in close proximity of each other can get even closer to form aggregated structures. TGA enables the correlation of residual weight of the solvent with the amount of bound solvent molecules [32]. As shown in Fig. 6, the residual weight of nanocomposites in the range of 90–

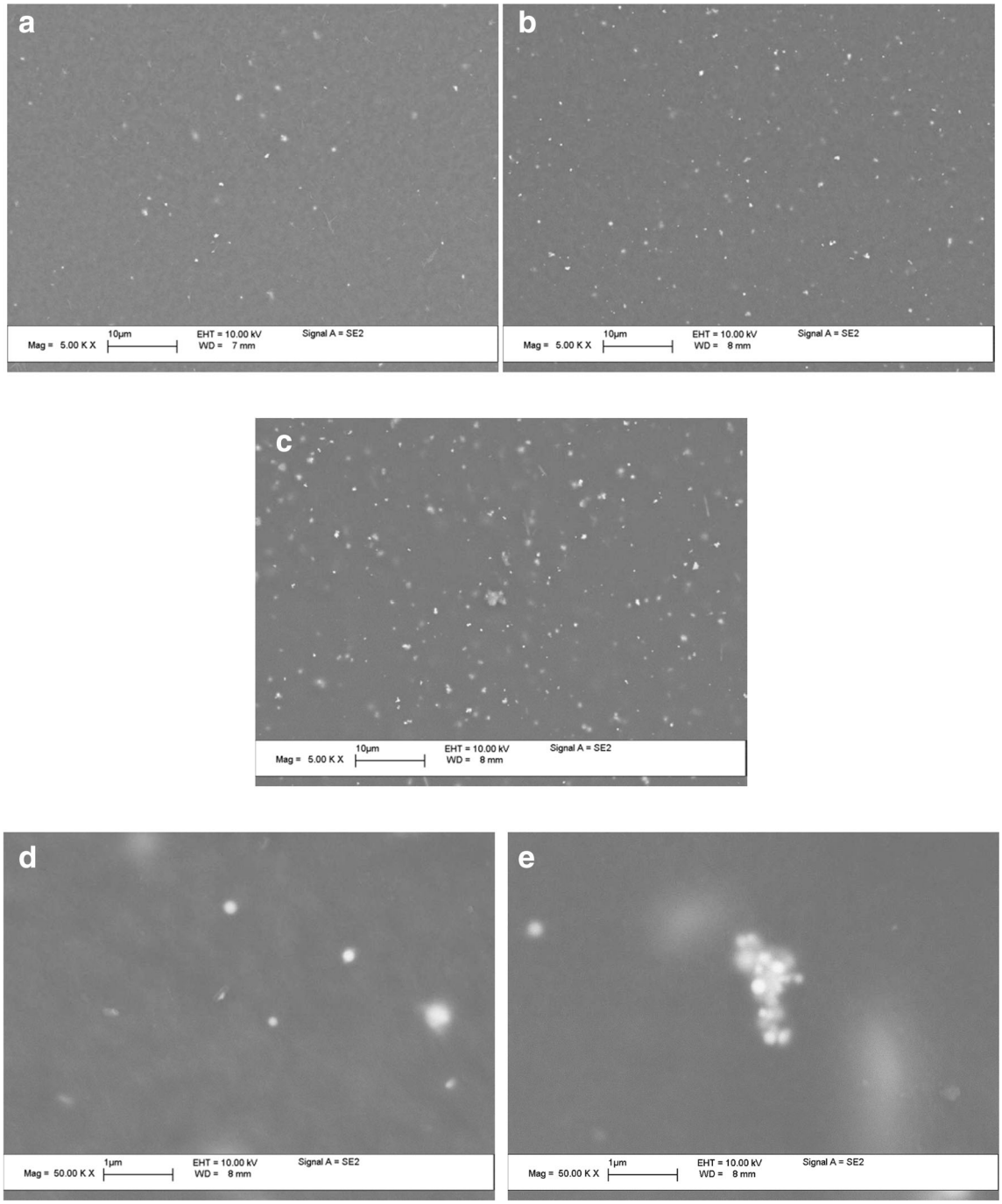

Fig. 4 SEM of nanocomposite films of **a** S1 (1 wt% filler), **b** S4 (4 wt% filler), and **c** S8 (8 wt% filler), high magnification SEM of **d** S4 and **e** S8

150 °C increased with Sb_2O_3 content up to 4 wt% and decreased beyond this point but not to lower values than that of the neat polymer solution (S0). Indeed, the shorter solvent bridges of stronger interactions tend to appear more frequently when nanoparticles are present in the solution. This observation is also in agreement with the dispersion state of nanoparticles—the well-dispersed nanocomposite (S4) presents more solvent bridges with stronger interactions than the nanocomposite with agglomerated filler particles (S8).

Extensional rheology

To monitor the lifetime of the filament, the change of midpoint diameter as a function of time for different solutions was measured (Fig. 7a). The filament of neat polymer solution (S0) ruptured within 7.9 s, while addition of Sb_2O_3 nanoparticles retarded the initial thinning process and increased the lifetime of the filament. The difference in the decay of the initial diameter is not pronounced, but the diameter at breakup point

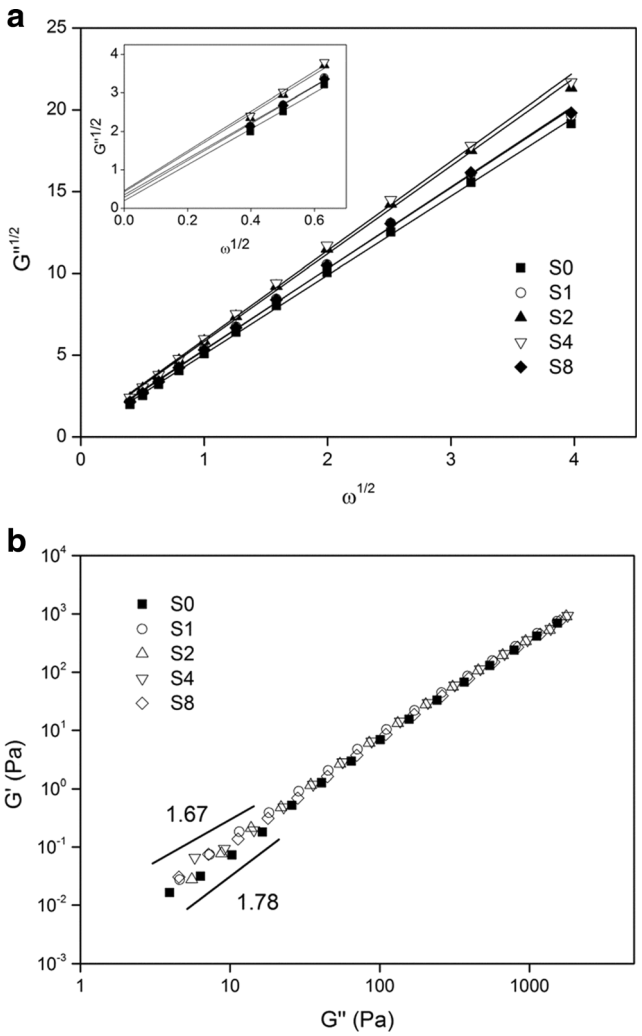

Fig. 5 **a** Plots of square root of loss modulus as a function of square root of frequency (*inset* magnifies the plots at $\omega^{1/2} < 0.7$) and **b** Cole–Cole plot of nanocomposites

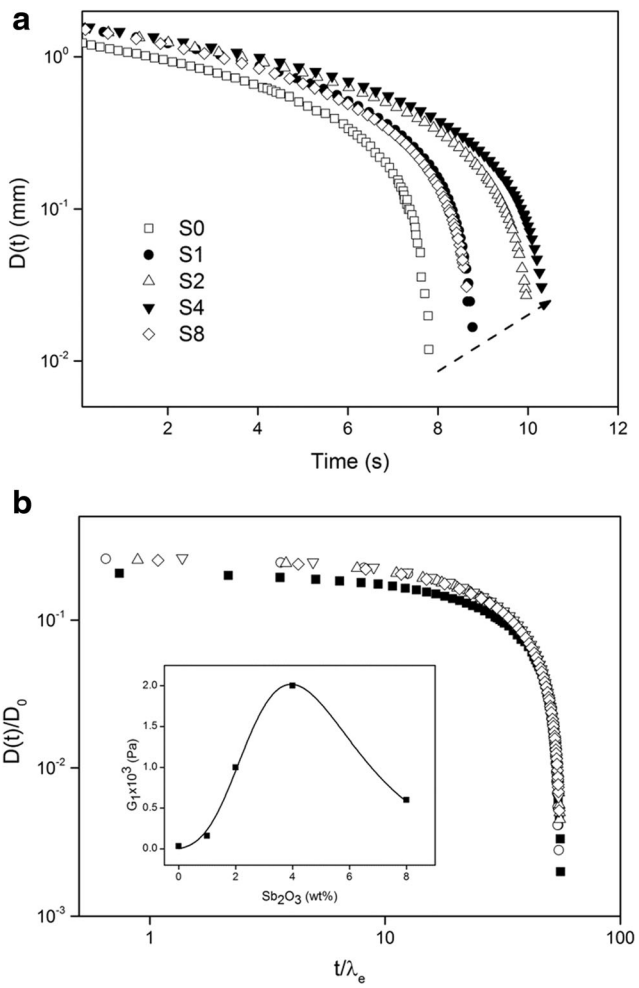

Fig. 7 **a** Change of midpoint diameter as a function of time and **b** master curve generated from the dimensionless midpoint diameter as a function of dimensionless time; *inset* shows values of elastic modulus determined by Eq. 2 at $t = t_1$

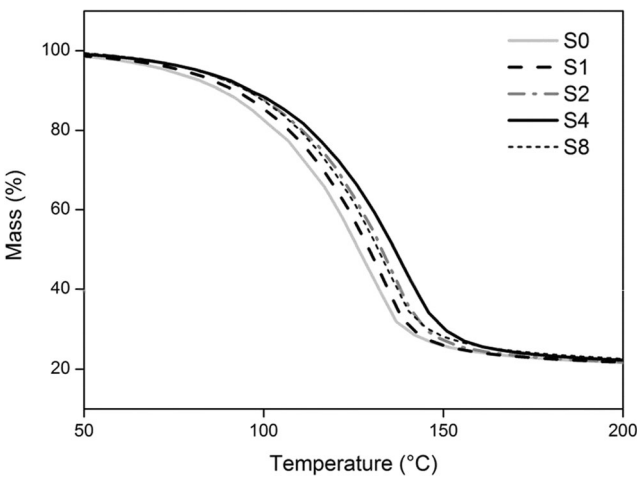

Fig. 6 TGA of PAN solutions with different amounts of Sb_2O_3 nanoparticles (the *inset* magnifies the change of mass the nanocomposites in the range of 160–200 °C)

increases with the filler content. All samples exhibited Newtonian behavior in low deformation times that is characterized by linear necking rate in time, followed by an exponential decrease of midpoint diameter (elastocapillary behavior) close to the breakup point. For a purely viscous liquid, the midpoint diameter decreases linearly with time according to Eq. 2 [37]:

$$D(t) = 0.0709\frac{2\sigma}{\eta_s}(t_c - t) \quad (2)$$

where η_s is viscosity (Pa s), σ is surface tension (N/m), and t_c is the capillary breakup time (s). However, for a polymer solution, diameter of the liquid bridge initially decreases predominantly under capillary-driven flow. During the thinning process, the deformation of microstructure forms an additional elastic stress, which grows exponentially with total strain. Consequently, in the terminal regime of the thinning process, the diameter decreases faster than linearly decaying regime

resulting in a downward curvature of the midpoint diameter vs. time curve in the semi-log plot. This behavior is generally attributed to the strain hardening of these solutions and the finite extensibility of the polymer chains [38, 39]. The change of midpoint diameter in elastocapillary thinning regime can be described as shown in Eq. 3 [19]:

$$\frac{D(t)}{D_0} = \left(\frac{G_1 D_0}{4\sigma}\right)^{1/3} \exp\left(-\frac{t-t_1}{3\lambda_e}\right) \quad (3)$$

where G_1 (Pa) is characteristic elastic modulus, t_1 (s) is the onset of elastocapillary region, and λ_e (s^{-1}) is the longest fluid relaxation time representing the onset of chain stretching in polymer solutions. By intersecting the lines that are fitted to linearly decaying and exponentially decaying (elastocapillary section) regimes, t_1 was determined, and λ_e was extracted by fitting the experimental points of elastocapillary thinning region ($t > t_1$) with Eq. 3. In addition, G_1 was found by using the diameter of filament at $t = t_1$ and rearrangement of Eq. 3. Increasing amount of Sb_2O_3 nanoparticles (up to 4 wt%) in polymer solution retarded the onset of elastocapillary region and shifted the diameter at the onset of this region ($D(t_1)$) to higher values. As listed in Table 2, the measured relaxation time is 140 ms in neat polymer solution, and it progressively increases with filler content.

Non-dimensionalizing of the midpoint diameter by D_0 and time by λ_e collapsed CaBER data points onto a master curve for times greater than the onset of the elastocapillary regime (Fig. 7b). In addition, characteristic elastic modulus was found to scale with the filler content up to 4 wt% (inset of Fig. 7b). However, S8 showed lower G_1 compared to that of S4 that is in agreement with the results of shear rheology and can be attributed to poor dispersion of the filler in PAN matrix (Fig. 5c, e).

Having the change in diameter of filaments as a function of time, strain rate (ε, s^{-1}) and thus apparent transient extensional viscosity (η_E, Pa s) can be described according to following equations [37, 38]:

$$\varepsilon = \frac{-2}{D(t)} \frac{\mathrm{d}D(t)}{\mathrm{d}t} \quad (4)$$

Table 2 Onset of the elastocapillary region (t_1), relaxation time (λ_e), diameter at t_1 ($D(t_1)$), and strain hardening (β) factor of all solutions

	t_1 (s)	λ_e (s)	$D(t_1)$ (mm)	β
S0	7.6	0.14	0.06	1.09
S1	8.1	0.16	0.11	1.06
S2	8.7	0.18	0.20	1.17
S4	8.8	0.19	0.26	1.19
S8	7.8	0.15	0.17	1.09

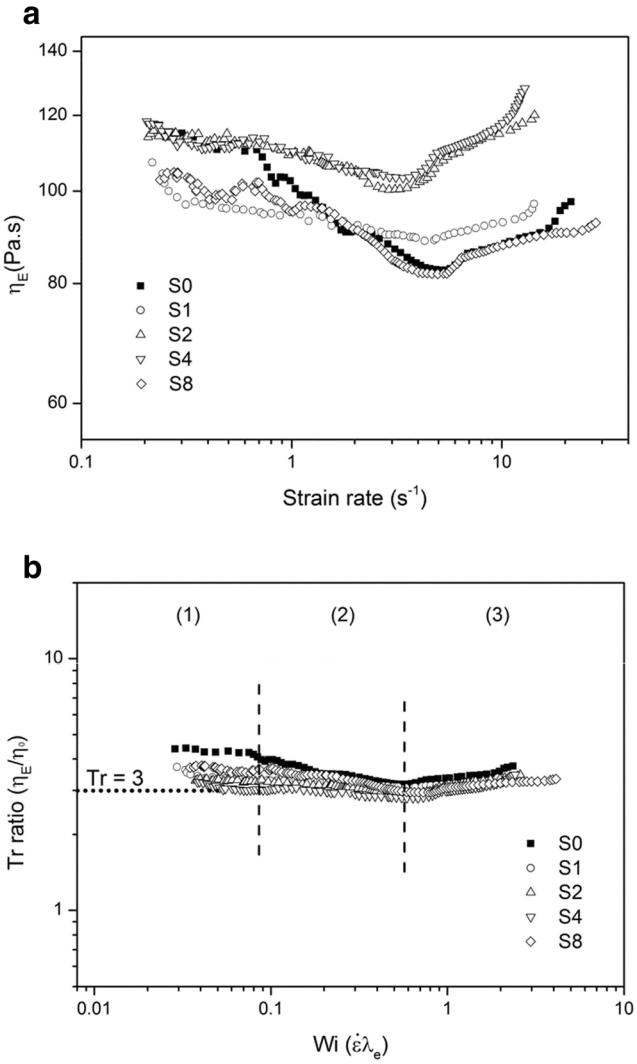

Fig. 8 **a** Extensional viscosity as a function of strain rate and **b** Trouton ratio as a function Hencky strain for different solutions

$$\eta_E = \frac{\Delta\tau(t)}{\varepsilon(t)} = -\frac{\sigma}{\frac{D(t)}{\mathrm{d}t}} \quad (5)$$

where $\Delta\tau(t)$ is total extensional stress difference in the elongating filament (Pa). Figure 8a shows extensional viscosity calculated by Eq. 5 against the strain rate for all solutions. The fluid column in CaBER is allowed to select its own necking rate due to the balance of capillary and elastic forces in response to the variation of viscosity, and this balance has significant effect on the extensional viscosity of the filament [40].

Three regimes can be observed in viscosity curve of a neat polymer solution; in regime one, viscosity is almost constant and is controlled by a visco-capillary balance of capillary pressure and viscous stresses in the filament. In regime 2, the chains become increasingly deformed, disentangled, and orientated whereby viscosity decreases

with $\dot{\varepsilon}$ (i.e., extensional thinning). In regime 3, viscosity grows with $\dot{\varepsilon}$ that is related to the extension of polymer coils as a result of the change of viscosity-dominated regime to elastocapillary thinning regime [39–41]. After the addition of Sb_2O_3 nanoparticles, overall shape of the viscosity curves, which contain three different regimes, remained similar in all nanocomposites. Minimal change of extensional viscosity was detected at low strain rates. On the other hand, larger extensional viscosity compared to neat polymer solution was observed at intermediate to high strain rates (in particularly S2 and S4). As a result, addition of Sb_2O_3 nanoparticles was found to develop plastic deformation zones in a controlled fashion that led to the stabilization of the filament for a longer time (Fig. 7a). In strong extensional flows, pure polymers can display strain-hardening behavior, which is defined as an increase of the extensional viscosity with deformation rate. Incorporation of fillers to polymer matrix typically enhances strain-hardening property as a result of longer relaxation time of the composite than that of the polymer host [42, 43]. On the other hand, it is known that adding particles can also reduce or suppress the strain-hardening and even produce extensional softening in polymer nanocomposites [43–45]. To quantify the effect of Sb_2O_3 nanoparticles on strain-hardening property, β parameter, which is defined as the ratio of extensional viscosity at high extensional rate to the extensional viscosity at critical strain rate where the strain hardening sets in, is used. In our system, strain rate of 12 s^{-1} was chosen as the upper limit to determine β, since it produces an adequate and comparable degree of strain-hardening in all solutions. As the strain-hardening property begins at the onset of the elastocapillary regions, the related strain rates were selected as the lower limit to specify β. As listed in Table 2, the addition of Sb_2O_3 nanoparticles first decreased β and then increased the strain-hardening parameter of nanocomposites. According to Meins et al. [42] and Handge et al. [44], the rigid particles cannot follow the externally applied extensional flow field. As polymer chains partially stick to the nanoparticles (Fig. 3a), the chains are less stretchable during elongation. This situation hinders slip between filler and the surrounding matrix and creates a complex flow near the nanoparticles that forms substantial shear components in a flow field (in addition to the elongational components). As a result, partial conversion from extensional to shear flow in the fluid interferes with the occurrence of strain-hardening and thus decreases the strain-hardening property in S1 compared to the neat polymer solution. While the change in characteristic elastic modulus of S1 compared to S0 is not significant (inset of Fig. 7b), the variation of β with filler content beyond 1 wt% follows the characteristic elastic modulus of nanocomposites (Table 1). These contributions suggest that the change in strain-hardening property of nanocomposites can be attributed to the interplay of the local shear components and elasticity of polymer matrix in the elastocapillary region. Therefore, the observation of maximum and minimum points in β versus filler content graph confirms the competition of intermolecular interactions and thus elasticity of polymer chains with generated shear component in the solutions.

To compare the rheological response of different solutions, extensional viscosity was normalized to Trouton ratio (Tr) by the use of the zero shear viscosity (Table 1) and extensional rate was non-dimensionalized to Weissenberg number (Wi) by the relaxation time (Table 2). The former shifts extensional viscosities vertically toward the Newtonian limit of $Tr = 3$, while the latter shifts the strain rates horizontally to an extent that depends on the choice of the relaxation time [41]. As presented in Fig. 8b, Tr values slightly decreased with filler content at $Wi < 0.1$ and became independent of the amount of nanoparticles at higher Wi numbers. Upturn point of Tr values was found to be 0.55 ± 0.05, which is in good agreement with $Wi = 0.5$ proposed by McKinley [37] for the start of the coil-stretch transition. In addition, Tr values of nanocomposites were lower than that of the neat polymer solution for entire range of Wi numbers. This result demonstrates that the addition of the filler leads to higher increase in shear viscosity than extensional viscosity.

Conclusion

PAN-based nanocomposites have been widely studied for various applications; however, the processability of these solutions has attracted less attention. Understanding the rheological behavior of PAN solutions, both in shear and elongational flow, forms a basis for the design of fiber-forming technologies. For the assessment of shear-free elongational flow—the simulation of the spinning process, we monitored change of elasticity, strain hardening, and viscosity through capillary breakup extensional rheometry. The change in elongational properties of solutions was related to the interplay of the local shear components and elasticity of the polymer matrix. The variations of shear rheological properties of nanocomposites were linked to trapping of polymer chains on the particles, enhanced physical structure of PAN domains in the solution, and dispersion state of the filler. We believe the structural phenomena that are systematically analyzed and related to the physical parameters in this work will shed light to choosing processing parameters in fiber-forming technologies.

Compliance with ethical standards

Conflict of interest The authors declare no conflict of interest.

Source of funding The authors declare no sources of funding.

References

1. Lu H, Wilkie CA (2010) Synergistic effect of carbon nanotubes and decabromodiphenyl oxide/Sb2O3 in improving the flame retardancy of polystyrene. Polym Degrad Stab 95(4):564–571. doi:10.1016/j.polymdegradstab.2009.12.011
2. M. Lewin SMA, E.M. Pearce (1978) Flame—retardant polymeric materials, vol 2. Plenum Press, New York
3. W.D. Schindler PJH (2004) Chemical finishing of textiles. Woodhead Publishing Limited, England
4. Li N, Xia Y, Mao Z, Wang L, Guan Y, Zheng A (2012) Influence of antimony oxide on flammability of polypropylene/intumescent flame retardant system. Polym Degrad Stab 97(9):1737–1744. doi:10.1016/j.polymdegradstab.2012.06.011
5. Si M, Feng J, Hao J, Xu L, Du J (2014) Synergistic flame retardant effects and mechanisms of nano-Sb2O3 in combination with aluminum phosphinate in poly(ethylene terephthalate). Polym Degrad Stab 100:70–78. doi:10.1016/j.polymdegradstab.2013.12.023
6. Rahaman MSA, Ismail AF, Mustafa A (2007) A review of heat treatment on polyacrylonitrile fiber. Polym Degrad Stab 92(8): 1421–1432. doi:10.1016/j.polymdegradstab.2007.03.023
7. Nataraj SK, Yang KS, Aminabhavi TM (2012) Polyacrylonitrile-based nanofibers—a state-of-the-art review. Prog Polym Sci 37(3): 487–513. doi:10.1016/j.progpolymsci.2011.07.001
8. Hall ME, Zhang J, Richard Horrocks A (1994) The flammability of polyacrylonitrile and its copolymers III. Effect of flame retardants. Fire Mater 18(4):231–241. doi:10.1002/fam.810180406
9. Tan L, Pan J, Wan A (2012) Shear and extensional rheology of polyacrylonitrile solution: effect of ultrahigh molecular weight polyacrylonitrile. Colloid Polym Sci 290(4):289–295. doi:10.1007/s00396-011-2546-1
10. Tan L, Liu S, Pan D (2009) Viscoelastic behavior of polyacrylonitrile/dimethyl sulfoxide concentrated solution during thermal-induced gelation. J Phys Chem B 113(3):603–609. doi:10.1021/jp809701b
11. Xu L, Qiu F (2015) Unusual viscosity behavior of polyacrylonitrile in NaSCN aqueous solutions. Polymer 64:130–138. doi:10.1016/j.polymer.2015.03.043
12. Zhang D, Karki AB, Rutman D, Young DP, Wang A, Cocke D, Ho TH, Guo Z (2009) Electrospun polyacrylonitrile nanocomposite fibers reinforced with Fe3O4 nanoparticles: Fabrication and property analysis. Polymer 50(17):4189–4198. doi:10.1016/j.polymer.2009.06.062
13. Newcomb BA, Chae HG, Gulgunje PV, Gupta K, Liu Y, Tsentalovich DE, Pasquali M, Kumar S (2014) Stress transfer in polyacrylonitrile/carbon nanotube composite fibers. Polymer 55(11):2734–2743. doi:10.1016/j.polymer.2014.04.008
14. Mataram A, Ismail AF, Mahmod DSA, Matsuura T (2010) Characterization and mechanical properties of polyacrylonitrile/silica composite fibers prepared via dry-jet wet spinning process. Mater Lett 64(17):1875–1878. doi:10.1016/j.matlet.2010.05.031
15. Liu X, Zhu C, Dong H, Wang B, Liu R, Zhao N, Li S, Xu J (2015) Effect of microgel content on the shear and extensional rheology of polyacrylonitrile solution. Colloid Polym Sci 293(2):587–596. doi:10.1007/s00396-014-3419-1
16. Akhlaghi O, Akbulut O, Menceloglu YZ (2015) Shear and extensional rheological characterization of poly(acrylonitrile)/halloysite nanocomposite solutions. Eur Polym J 73:17–25. doi:10.1016/j.eurpolymj.2015.09.022
17. Chen B, Evans JRG, Greenwell HC, Boulet P, Coveney PV, Bowden AA, Whiting A (2008) A critical appraisal of polymer-clay nanocomposites. Chem Soc Rev 37(3):568–594. doi:10.1039/B702653F
18. Du W, Chen H, Xu H, Pan D, Pan N (2009) Viscoelastic behavior of polyacrylonitrile/dimethyl sulfoxide concentrated solution with water. J Polym Sci B Polym Phys 47(15):1437–1442. doi:10.1002/polb.21743
19. Haward SJ, Sharma V, Butts CP, McKinley GH, Rahatekar SS (2012) Shear and extensional rheology of cellulose/ionic liquid solutions. Biomacromolecules 13(5):1688–1699. doi:10.1021/bm300407q
20. A.R. Horrocks SCA (2000) Handbook of Technical Textiles. Woodhead Publishing Limited, England
21. Cassagnau P (2003) Payne effect and shear elasticity of silica-filled polymers in concentrated solutions and in molten state. Polymer 44(8):2455–2462. doi:10.1016/S0032-3861(03)00094-6
22. Jeon HS, Rameshwaram JK, Kim G, Weinkauf DH (2003) Characterization of polyisoprene–clay nanocomposites prepared by solution blending. Polymer 44(19):5749–5758. doi:10.1016/S0032-3861(03)00466-X
23. Shen L, Lin Y, Du Q, Zhong W, Yang Y (2005) Preparation and rheology of polyamide-6/attapulgite nanocomposites and studies on their percolated structure. Polymer 46(15):5758–5766. doi:10.1016/j.polymer.2005.05.040
24. Cassagnau P (2008) Melt rheology of organoclay and fumed silica nanocomposites. Polymer 49(9):2183–2196. doi:10.1016/j.polymer.2007.12.035
25. Yin H, Chen H, Chen D (2010) Viscoelastic behavior of poly(acrylonitrile)/attapulgite nanocomposite solution. Colloids Surf A Physicochem Eng Asp 367(1–3):52–59. doi:10.1016/j.colsurfa.2010.06.017
26. Krishnamoorti R, Vaia RA, Giannelis EP (1996) Structure and dynamics of polymer-layered silicate nanocomposites. Chem Mater 8(8):1728–1734. doi:10.1021/cm960127g
27. Lee KM, Han CD (2003) Effect of hydrogen bonding on the rheology of polycarbonate/organoclay nanocomposites. Polymer 44(16):4573–4588. doi:10.1016/S0032-3861(03)00444-0
28. Miyoshi E, Nishinari K (1999) Non-Newtonian flow behaviour of gellan gum aqueous solutions. Colloid Polym Sci 277(8):727–734. doi:10.1007/s003960050446
29. Cosgrove T, Roberts C, Choi Y, Schmidt RG, Gordon GV, Goodwin AJ, Kretschmer A (2002) Relaxation studies of high molecular weight poly(dimethylsiloxane)s blended with polysilicate nanoparticles. Langmuir 18(26):10075–10079. doi:10.1021/la025883h
30. Lecouvet B, Sclavons M, Bourbigot S, Devaux J, Bailly C (2011) Water-assisted extrusion as a novel processing route to prepare polypropylene/halloysite nanotube nanocomposites: structure and properties. Polymer 52(19):4284–4295. doi:10.1016/j.polymer.2011.07.021
31. Lecouvet B, Gutierrez JG, Sclavons M, Bailly C (2011) Structure–property relationships in polyamide 12/halloysite nanotube nanocomposites. Polym Degrad Stab 96(2):226–235. doi:10.1016/j.polymdegradstab.2010.11.006
32. Eom Y, Kim BC (2014) Solubility parameter-based analysis of polyacrylonitrile solutions in N, N-dimethyl formamide and dimethyl sulfoxide. Polymer 55(10):2570–2577. doi:10.1016/j.polymer.2014.03.047
33. Lyoo WS, Kim JH, Choi JH, Kim BC, Blackwell J (2001) Role of degree of saponification in the shear-induced molecular orientation of syndiotacticity-rich ultrahigh molecular weight poly(vinyl alcohol). Macromolecules 34(12):3982–3987. doi:10.1021/ma001338g
34. Lyoo WS, Yeum JH, Kwon OW, Shin DS, Han SS, Kim BC, Jeon HY, Noh SK (2006) Rheological properties of high molecular weight (HMW) syndiotactic poly(vinyl alcohol) (PVA)/HMW atactic PVA blend solutions. J Appl Polym Sci 102(4):3934–3939. doi:10.1002/app.24223
35. Tan L, Liu S, Pan D, Pan N (2009) Gelation of polyacrylonitrile in a mixed solvent: scaling and fractal analysis. Soft Matter 5(21):4297–4304. doi:10.1039/B911635D

36. Tan L, Pan D, Pan N (2009) Rheological study on thermal-induced gelation behavior of polyacrylonitrile solution. J Polym Res 16(4): 341–350. doi:10.1007/s10965-008-9234-y
37. McKinley GH (2005) Visco-elasto-capillary thinning and break-up of complex fluids. In. Rheology Reviews, p 1–48
38. McKinley GH, Tripathi A (2000) How to extract the Newtonian viscosity from capillary breakup measurements in a filament rheometer. J Rheol 44(3):653–670. doi:10.1122/1.551105
39. Kheirandish S, Gubaydullin I, Willenbacher N (2009) Shear and elongational flow behavior of acrylic thickener solutions. Part II: effect of gel content. Rheol Acta 48(4):397–407. doi:10.1007/s00397-008-0324-x
40. Anna SL, McKinley GH (2001) Elasto-capillary thinning and breakup of model elastic liquids. J Rheol 45(1):115–138. doi:10.1122/1.1332389
41. Sridhar T, Acharya M, Nguyen DA, Bhattacharjee PK (2014) On the extensional rheology of polymer melts and concentrated solutions. Macromolecules 47(1):379–386. doi:10.1021/ma401213r
42. Le Meins J-F, Moldenaers P, Mewis J (2003) Suspensions of monodisperse spheres in polymer melts: particle size effects in extensional flow. Rheol Acta 42(1–2):184–190. doi:10.1007/s00397-002-0270-y
43. Takahashi T, J-i T, Koyama K (1999) Uniaxial elongational viscosity of various molten polymer composites. Polym Compos 20(3): 357–366. doi:10.1002/pc.10362
44. Handge UA, Pötschke P (2007) Deformation and orientation during shear and elongation of a polycarbonate/carbon nanotubes composite in the melt. Rheol Acta 46(6):889–898. doi:10.1007/s00397-007-0179-6
45. Uematsu H, Aoki Y, Sugimoto M, Koyama K (2011) Rheology of SiO 2 /(acrylic polymer/epoxy) suspensions. III. Uniaxial elongational viscosity. Rheol Acta 50(5–6):433–439. doi:10.1007/s00397-010-0509-y